

# A parametric study of the pipeline hammer phenomenon in plastic Bingham slurry flows using the finite element method

Felipe Galarce<sup>1\*</sup> and Francisco Martinez<sup>1†</sup>

<sup>1\*</sup>School of Civil Engineering, Pontificia Universidad Católica de Valparaíso, Avenida Brasil 2147, Valparaiso, 2340000, Chile.

\*Corresponding author(s). E-mail(s): [felipe.galarce@pucv.cl](mailto:felipe.galarce@pucv.cl);

Contributing authors: [francisco.martinez@pucv.cl](mailto:francisco.martinez@pucv.cl);

†These authors contributed equally to this work.

## Abstract

We do a numerical study of the transient phenomenon in pipelines transporting plastic Bingham slurry flows, using a lowest-order finite element method (FEM). While most pipeline hammer studies focus on Newtonian fluids, the transient dynamics in Bingham fluids remains elusive and poorly afforded, even though this case has significant impact in industry like mining. A detailed parametric study assesses the effects of the slurry yield stress and the valve closure times on both, pressure and velocity distributions along the pipeline, using an adaptive friction model to account for turbulent slurries. Results reveal that yield stress enhances flow resistance and accelerates pressure peak attenuation, underscoring the damping role of Bingham rheology compared to Newtonian flows. These insights emphasize the need for advanced FEM-based schemes in non-Newtonian shockwave modeling, with implications for industrial pipeline design and operational safety.

**Keywords:** pipeline hammer, finite elements method, plastic Bingham fluid, rheological effects, downstream closure model, slurry flows

## 1 Introduction

Water-hammer is a common and critical phenomenon in many hydro-transport systems around the world. This problem is often caused by sudden operations in transport systems, such as a sudden closing or opening of flow control valves, pump or turbines power outages, or the pipeline ruptures, to name a few examples [1]. These events can generate intense pressure shockwaves traveling along the pipeline at very high speeds, covering long distances in quite short times. This feature gives very short time for a mechanical response to the pipeline walls, resulting in a significant increase in flow's pressure and, in extreme cases, approaching to the limit mechanical strength of the pipeline. Then, this is a significant challenge for the operation of pipelines including system's failure, equipment damage and operational inefficiencies, among other [2].

The hydraulic modeling of water-hammer has been intensely studied for Newtonian fluids, particularly for water transportation systems [3, 4]. However, an opposite situation occurs when dealing with complex fluids where few studies can be found [5–9]. Non-Newtonian fluids are frequently encountered in mining industry, exhibiting operational problems similar to those found in water pipelines. The transport of slurries and mineral concentrates (e.g., copper tailings) and in general, solid-liquid suspensions of higher concentrations are good examples of rheological complex fluids, with both commercial interest and environmental impact [10–13].

Recent studies have addressed this phenomenon affording specific topics such as shear-thinning, shear-thickening or even tixotropy effects on shockwave propagation [14], missing an overall analysis about the influence of physical-mechanical parameters on the transient evolution on these flows. The complexity of the modeling

of solid-liquid flows is usually related to the rheological character of the flow, often exhibiting a mechanical behavior similar to the plastic Bingham model. This model is particularly present for volume concentrations up to  $C_V \approx 30\%$  [15]. A dramatic increase in this concentration could lead to hyperconcentrated regimes governed by nonlinear rheological models [16–18].

On the other hand, mining tailings are usually characterized by viscosity values ( $\eta$ ) up to 100 times higher than the viscosity of water and the existence of yield stress ( $\tau_y$ ) affecting the initial mobility of the mixture [15, 19]. If flow’s pressure and inertia are not able to overcome  $\tau_y$ , no flow is possible. Then it is clear that viscosity ( $\eta$ ) and yield stress could lead to different dynamics with respect to classical water-hammer phenomenon, affecting the magnitude of the pressure wave, the shockwave speed and the attenuation dynamics [20].

Current state of the art on the water-hammer numerical modeling includes several approaches, ranging on different trades-off between computational cost and accuracy. First, computational fluid dynamics (CFD) offer detailed simulations of transient evolution by directly solving the Navier-Stokes equations [21]. CFD models capture complex transient characteristics including shock waves, column separation and fluid-structure interaction. Advanced CFD tools incorporate adaptive mesh refinement, multi-phase flow modeling, and coupling with structural analysis to predict the response of piping systems and components accurately [22]. Second, hybrid approaches combine the detailed flow dynamics captured by CFD codes with the computational efficiency of 1D models [23].

These models are useful for analyzing systems where local three-dimensional effects are significant, although the overall behaviour of the event can be approximated as 1D [24]. Hybrid models enable detailed analysis of specific components (e.g., pump or valve regions) while efficiently analyzing the broader system. Finally, machine learning and artificial intelligence (AI) simulation techniques is gaining growing interest to predict and mitigate water hammer effects [25]. These approaches can identify patterns from historical data, simulate various operational scenarios, and recommend preventive or mitigation strategies. Machine learning models can complement traditional simulation methods by providing insights derived from large datasets that are impractical to analyze with conventional methods [26].

## 1.1 One dimensional models

One-dimensional (1D) models are among the most popular schemes for water-hammer analysis. Often based on the method of characteristics (MOC) (e.g. [1, 24]), they can efficiently simulate shockwave propagation in pipes accounting for wall shear stress and friction, simplified flow-structure interaction models, presence of bifurcations or valve closure models, among others. Recent progress have improved the accuracy and computational cost of these models allowing for the simulation of large hydraulic systems. This approach becomes interesting when dealing with mining suspensions, considering the difficulty of solving the coupled motion equations associated to the solid and liquid phases [27, 28], but also because of the dynamical relations involved on the interaction between both phases require previous empirical validation which is not always available. The continuous modeling of pipeline hammer incorporating a rheological model emerges then as a simple and low-cost alternative for predicting pressure impacts in a pipe.

In this context, this research aims to address the transient dynamics when dealing with plastic Bingham flows in horizontal, single diameter elastic-walled pipelines. Recent works have numerically afforded this case, studying the pressure waves generated after a sudden valve closure in a pipeline with Bingham fluids flows [24, 29, 30], but also in power-law fluids [31]. Although these studies have reached significant progress, there are still several gaps that need to be addressed. By one hand, a better understanding on the influence of rheological parameters (e.g.,  $\eta$ ,  $\tau_y$ ) on the propagation of pressure waves, changes in flow friction, water-hammer attenuation is required. On the other hand, the effects induced by gradual operations of some flow control instruments (e.g., valves), is also needed. This kind of operations obviously affect the decay dynamics of flow’s velocity and pressure, the most important variables in the pipelines operation.

In our case, a methodological difference concerning the spatial discretization of the governing dynamics of the system was considered. The gold standard has relied on the method of characteristics [2, 24] with a structured

2D grid for space and time. Taking into account the consolidated computational power of the last decades, we consider instead a finite element approach which allows one not only to solve the classical conservation equations, but also to extend them to several other scenarios. With classical MOC, the hypothesis of quasi-linearity must be ensured, meaning that the equations terms must be either linear or depend solely on the unknown but not its derivatives.

This paper is organized as follows: first, the governing equations for non-Newtonian transient phenomenon are introduced, showing its dimensionless form and the computation of Bingham friction factors. Then, the numerical scheme used to handle the equations in time and space is also described. Next, we show numerical experiments we have conducted to: first, test space and time convergence for the FEM scheme we use, second, to simulate a realistic copper slurry, third, to test out several yield stress configurations and asses their impact on the overall dynamics, and fourth, to asses the valve closure time impact on the pressure wave evolution and peak values.

## 2 Governing Equations

Hydraulic transient equations for pipes are widely covered in literature, particularly for water transport. However, for non-Newtonian fluids like Bingham fluids or other complex rheologies, the available literature is much scarcer. In this context, we use a standard formulation for slurry flows [24], used to model a pipe hammer with Bingham fluids in laminar systems of constant internal diameter and constant upstream head pressure. We include a friction model accounting for the laminar and turbulent hydrodynamic character of the flow, several alternatives for the valve closure model, and also the convective effects contained in the term  $u\partial u/\partial x$ , usually neglected in this kind of simulations.

In this article, the pressure and velocity wave propagation after the closure of a control valve at the pipeline downstream section, is modeled as depicted in Figure 2. In this setup, an upstream head reservoir of height  $H$  is connected to the pipe of inner diameter  $D$  and total length  $L$ . A control valve is located at the downstream section of the system, which can close instantaneously ( $T = 0$ ) or gradually ( $T > 0$ ) depending on the operating conditions, where  $T$  is the closure time. The condition  $T = 0$  is usually considered the most adverse scenario for pipeline safety. In this context, the one-dimensional (1D) averaged momentum and mass balance equations reads:

$$\left\{ \begin{array}{ll} \frac{\partial p}{\partial t} + \rho_m c^2 \frac{\partial u}{\partial x} = 0 & \text{in } (x, t) \in [0, L] \times [0, T], \\ \rho_m \left( \frac{\partial u}{\partial t} + u \frac{\partial u}{\partial x} \right) + \frac{\partial p}{\partial x} + \mathcal{S}(u) = 0 & \text{in } (x, t) \in [0, L] \times [0, T], \\ u = g(t) & \text{on } x = L, t \geq 0, \\ p = P_o := \rho_m g H & \text{on } x = 0, t \geq 0, \\ p = P_o \left( 1 - \frac{x}{L} \right) & \text{at } t = 0, x \in [0, L], \\ u = \frac{16}{f\widetilde{\text{Re}}} U_o & \text{at } t = 0, x \in [0, L], \end{array} \right. \quad (2.1)$$

where  $\eta$  is the fluid Bingham viscosity and  $\rho_m$  stands for the fluid density, which is understood as a mixture density for a bi-phasic media, as it will be explained later on. The parameters  $P_o, U_o$  stand for a characteristic pressure and a characteristic velocity, respectively. Namely, we set  $P_o = \rho_m g H$  and  $U_o$  as the stationary laminar flow mean velocity before the valve closure:

$$U_o := \frac{P_o D^2}{32 L \eta},$$

The reader may notice in the fore-coming sections that some simulations will surpasses the laminar regime. We will still admit  $U_o$  as a rough approximation for the 1D velocity initial condition. In addition, notice the corrector term sometimes called *conductance*,  $16/(f\widetilde{\text{Re}})$ , which accounts for the non-Newtonian behavior of the fluid. Notice as well that  $P_o$  is chosen as the boundary condition for the pressure at the head tank (at  $x = 0$ ), whereas a linear stationary profile is used for the pipeline pressure distribution accordingly with the

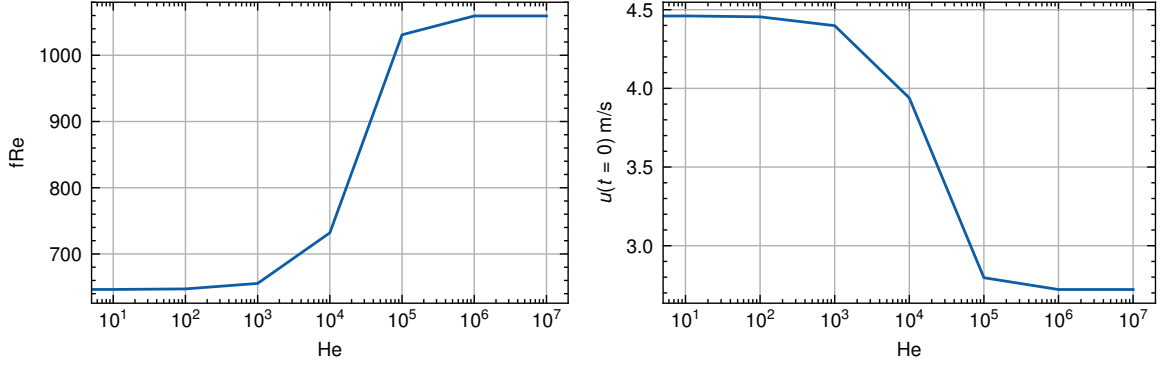


**Fig. 1** Initial conditions for the slurry system according to the parameter setup of a copper mixture, detailed in table 1

aforementioned initial condition for the velocity. Last, the valve closure model is described by a time-dependent function  $g(t)$  at  $x = L$ .

The parameter  $c$  represents the shockwave celerity. In addition,  $\widetilde{Re} = \frac{\rho U_o D}{\eta}$  stands for a reference Reynolds number computed with the characteristic velocity. These scales will be used later on to formulate the dimensionless form of the governing equations. In addition, an isothermic assumption is considered for the fluid compressibility leading to a constant value for the pressure wave speed  $c$ . Therefore, the equations describe a fluid flow with mixture density  $\rho_m$ , axial velocity  $u$ , pressure  $p$  and a reaction term denoted by  $\mathcal{S}(u)$ . This last term models the wall shear stress effect on the overall motion. Using the Fanning friction factor  $f$  [32], the cross-section velocity  $u$  and pipe diameter  $D$  we can write  $\mathcal{S}(u)$  as follows ([2], chapter 2):

$$\mathcal{S}(u) = \frac{2f\rho_m|u|u}{D} \quad (2.2)$$

The fluid rheology is implicit in this system through the friction coefficient. For instance, for Bingham flows the coefficient  $fRe$  can be readily estimated from the following relations [33, 34]:

$$fRe = \begin{cases} 16 + \frac{10.67 + 0.1414 \left(\frac{He}{Re}\right)^{1.143}}{1 + 0.0149 \left(\frac{He}{Re}\right)^{1.16}} \left(\frac{He}{4Re}\right), & Re < Re_c, \\ Re \left(\frac{10^a}{4Re^{0.193}}\right), & Re \geq Re_c \end{cases} \quad (2.3)$$

where  $a = -1.47(1 + 0.146 \exp(-2.9 \cdot 10^{-5} He))$  is an empirical coefficient [15]. Notice that these relations recover the Newtonian behavior when  $He = 0$ . The Reynolds ( $Re$ ) and Hedstrom ( $He$ ) numbers are introduced as follows [15]:

$$\begin{aligned} Re &= \frac{\rho D u}{\eta} \\ He &= \frac{\rho D^2 \tau_y}{\eta^2} \end{aligned} \quad (2.4)$$

where  $\tau_y$  is the yield stress and  $\eta$  the Bingham viscosity. The reader should notice that the system initial condition will heavily depend on both, the Reynolds and the Hedstrom number. For turbulent regimes, higher friction factors will be computed, thus leading to  $16/(fRe) \ll 1$ . A similar phenomena will be depicted for large Hedstrom numbers, where high yield-stresses will naturally lead a larger friction with the walls. In Figure 1, we show the starting conditions for friction and velocity of the system, for a range of Hedstrom numbers, using the parameter setup from 1. The reader should remark that the friction factor is a non-constant parameter in the simulation, thus increasing the overall numerical scheme as it is necessary to recompute the factor  $fRe$  at each time-step, in each mesh node.

## 2.1 Wave propagation on homogeneous mixtures

Among the assumptions made in this study, we will consider that the fluid is an homogeneous mixture, that is, a fluid whose solid concentration and velocity distribution can be considered practically uniform across the pipe diameter [15, 19]. The density of an homogeneous mixture ( $\rho_m$ ) is defined as [19]:

$$\rho_m = \rho_s C_V + \rho_f (1 - C_V) \quad (2.5)$$

where  $\rho_s, \rho_f$  denotes the solid and fluid densities, respectively and  $C_V$  the solid volumetric concentration. Theoretical estimations of the pressure surge  $\Delta P$  caused by a sudden change in the velocity regime in a pipeline it's a longstanding engineering challenge. Joukowski was the first to determine the pressure rise generated in a rigid-walled pipe transporting a Newtonian liquid of density  $\rho$  [35, 36], that is:

$$\Delta P = \rho_m c U_o \quad (2.6)$$

where  $U_o$  is the initial mean velocity just before the close of the valve,  $c$  is the shockwave speed. Since  $c \gg U_o$ , the wave speed is usually considered independent on the initial flow velocity. A general expression for the shockwave speed valid for incompressible, Newtonian liquids in single-diameter tubes, can be written as follows:

$$c = \sqrt{\frac{K_f}{\rho_f} \frac{1}{1 + \zeta}} \quad (2.7)$$

where  $K_f$  is the liquid bulk modulus. According to Young [37], for rigid walls pipelines we have  $\zeta = 0$ , and Korteweg shown [38, 39] that  $\zeta = 1 + \frac{K_f D}{E e}$  for elastic walls tubes, where  $E$  is the pipe elastic modulus,  $D$  the inner diameter of the tube and  $e$  the wall thickness. Other expressions considering pipe constraints can be found in Chaudhry [2]. The previous formulas can be adapted for estimating the wave speed celerity  $c_m$  for homogeneous and heterogeneous solid-liquid mixtures. In the former, the expression reported by Young can be simply adapted as follows:

$$c = \sqrt{\frac{K_m}{\rho_m}} \quad (2.8)$$

where  $K_m, \rho_m$  denotes the bulk modulus and mixture density, respectively. A way for estimating  $K_m$  is similar to Eq. (2.5), that is  $K_m = K_s C_V + K_f (1 - C_V)$ , where  $K_s$  is the bulk modulus of the slurry solid phase. The Korteweg law can also be written for solid-liquid mixtures as follows [7]:

$$c = \sqrt{\frac{\frac{K_m}{\rho_m}}{1 + \frac{K_m D}{E e}}} \quad (2.9)$$

where  $e$  stands for the wall thickness. Finally, another expression also valid for homogeneous mixtures and that considers the volumetric solid concentration  $C_V$ , reads [40, 41]:

$$c = \sqrt{\frac{\frac{K_f}{\rho_m}}{1 - C_V + \frac{K_f}{K_s} C_V + \frac{D}{e} \frac{K_f}{E}}} \quad (2.10)$$

In our numerical experiments, we will conduct simulations with this last expression, as it will be made clear in section 3.2.

## 2.2 The transition velocity for Bingham flows

The parameter  $Re_c = \rho u_c D / \eta$  from (2.3), can be considered as a critical flow Reynolds number indicating the laminar-turbulent separation regime. Such separation occurs at the velocity  $u_c$ , also called *transition velocity*

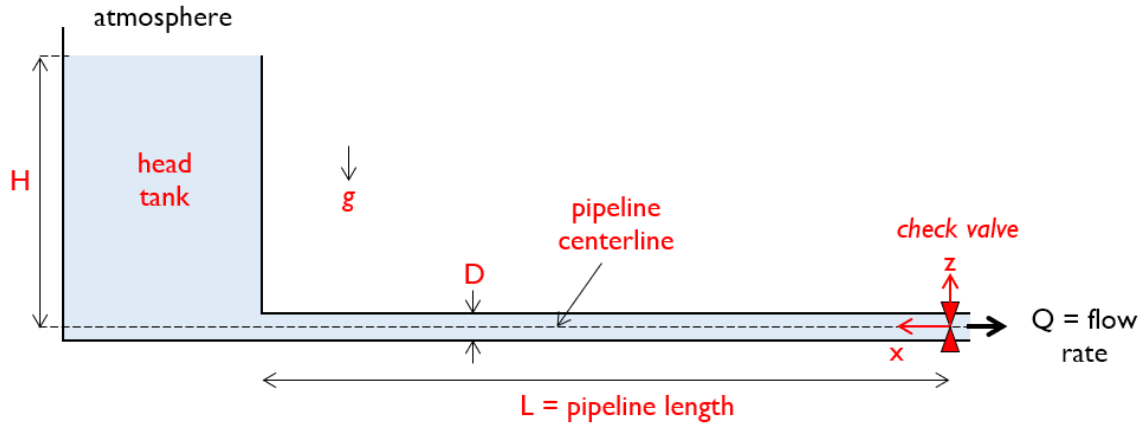


**Fig. 2** Scheme used for pipeline hammer analysis. The main flow and pipe variables are defined. The head tank is open to atmosphere and flow is one dimensional for all purposes.

[19]. When  $u < u_c$  the flow regime is laminar, and turbulent when  $u > u_c$ . This critical parameter can be determined by following the method proposed by Hanks and Pratt [15]:

$$\text{Re}_c = \frac{\text{He}}{X_c} \left( 1 - \frac{4}{3}X_c + \frac{1}{3}X_c^4 \right) \quad (2.11)$$

where  $X_c = \tau_y/(\tau_w)_c$ , and  $(\tau_w)_c$  is the critical wall shear stress. Just at the laminar-transition point Hanks proposed:

$$\text{He} = 16800 \frac{X_c}{(1 - X_c)^3} \quad (2.12)$$

This means we can compute the critical velocity and therefore the transition number  $\text{Re}_c$  fixing a Hedstrom number, thus allowing us to study several rheological behaviors of the flow. Remark as well that  $X_c$  can be physically interpreted as a Bingham number  $\text{Bi} = \tau_y/(\tau_w)_c$  for a fully developed Bingham flow, which is the only regime in which this relation is valid. For the Newtonian case, the threshold value  $\text{Re}_c = 2100$  will be employed following [42].

### 2.3 Dimensionless equations

The system given in Eq.(2.1) can be expressed in dimensionless form by introducing relevant characteristic scales for the velocity ( $U_o$ ), pressure ( $P_o$ ), position ( $L_o$ ) and time ( $T_o$ ) [24, 29, 30]. The scales for velocity and pressure were already introduced in the system (2.14). Exploiting the simplicity of the experimental setup, the time scale is chosen as  $T_o = L/c$ , for  $L_o = L$ . These definitions leads to the unknowns  $x^*, t^*, u^*, p^*$  defined as:

$$x^* = \frac{x}{L_o} = \frac{x}{L} \quad (2.13a)$$

$$t^* = \frac{t}{T_o} = \frac{tc}{L} \quad (2.13b)$$

$$p^* = \frac{p}{P_o} = \frac{p}{\rho g H} \quad (2.13c)$$

$$u^* = \frac{u}{U_o} = u \frac{32 \eta L}{P_o D^2} \quad (2.13d)$$

which leads to the following system of equations:

$$\left\{ \begin{array}{ll} \frac{\partial p^*}{\partial t^*} + \lambda_1 \frac{\partial u^*}{\partial x^*} = 0 & \text{in } (x^*, t^*) \in [0, 1] \times [0, T^*], \\ \lambda_1 \frac{\partial u^*}{\partial t^*} + \lambda_2 u^* \frac{\partial u^*}{\partial x^*} + \frac{\partial p^*}{\partial x^*} + \frac{f\text{Re}}{16} u^* = 0 & \text{in } (x^*, t^*) \in [0, 1] \times [0, T^*], \\ u^* = g^*(t) & \text{on } x^* = 1, t^* \geq 0, \\ p^* = 1 & \text{on } x = 0, t^* \geq 0, \\ p^* = 1 - x^* & \text{at } t^* = 0, x^* \in [0, 1], \\ u^* = \frac{16}{f\widetilde{\text{Re}}} & \text{at } t^* = 0, x^* \in [0, 1], \end{array} \right. \quad (2.14)$$

and where we have introduced,

$$\lambda_1 = \frac{\delta}{32} \widetilde{\text{Re}} \widetilde{\text{Ma}}^{-1} \quad (2.15a)$$

$$\lambda_2 = \frac{\delta}{32} \widetilde{\text{Re}} \quad (2.15b)$$

where  $\widetilde{\text{Ma}} = U_o/c$  is a reference Mach number defined with the stationary velocity  $U_o$ , and  $\delta = D/L$  is an aspect ratio for the pipeline geometry.

## 2.4 A lowest-order finite element formulation for slurry flows

Traditionally, 1D hammer dynamics have been solved by means of the Method of Characteristics (MOC). The MOC transforms the partial differential equations (PDEs) into ordinary differential equations (ODEs) along characteristic lines, which represent the paths along which wave information travels through the fluid. This method allows for the accurate simulation of wave propagation, reflection, and interaction within the pipeline system. Nevertheless, MOC relies upon restrictive hypothesis for the underlying model that force a set of boundaries for the applications to be tackled. For a system of continuous equations to be addressed with MOC, it is mandatory to satisfy quasi-linear conditions, meaning that in the equations one can allow either linear terms or, at most, terms that depends solely on the unknowns magnitude and not their derivatives. This is of relevance, for instance, whenever it is desired to solve the system considering complex friction models.

Among the alternatives to perform to numerically solve in space and time the equations (2.14) we can name the MOC [24], finite volumes [43], and the finite element method (FEM, [44] [45]). We will use the later to deal with space discretization and implicit finite differences for time. Let us consider a one-dimensional working domain, a straight line represented by the real interval  $\Omega = [0, L]$  ( $L \in \mathbb{R}$ ). In order to properly expose the numerical setup, it is required to formalize the functions  $u^* : [0, L] \rightarrow \mathbb{R}$  and  $p^* : [0, L] \rightarrow \mathbb{R}$  as an element of a Hilbert space  $\mathcal{H} = H^1([0, L]) \times L^2([0, L])$ , where  $L^2 = \{v : \Omega \rightarrow \Omega : \int_{\Omega} |v|^2 dx < \infty\}$ , and  $H^1(\Omega)$  stands for the smaller space of smoother functions  $H^1 = \{v \in L^2(\Omega); \partial v / \partial x \in L^2(\Omega)\}$ .

Under this setting, it is well known that one can reformulate the problem with a variational formulation, boiling the challenge down to finding a set of functions  $(u^{*,n+1}, p^{*,n+1}) \in \mathcal{H}$ , such that:

$$\begin{aligned} & \frac{1}{\Delta t} \int_{\Omega} p^{*,n+1} q dx + \lambda_1 \int_{\Omega} \frac{\partial u^{*,n+1}}{\partial x^*} q dx + \frac{\lambda_1}{\Delta t} \int_{\Omega} u^{*,n+1} w dx + \int_{\Omega} \frac{\partial p^{*,n+1}}{\partial x^*} w + \\ & + \lambda_2 \int_{\Omega} u^* \frac{\partial u^*}{\partial x^*} w dx + \frac{f\text{Re}}{16} \int_{\Omega} u^{*,n+1} w dx = \frac{1}{\Delta t^*} \int_{\Omega} p^{*,n} q dx + \frac{\lambda_1}{\Delta t^*} \int_{\Omega} u^{*,n} w dx, \end{aligned} \quad (2.16)$$

for all  $q \in L^2(\Omega)$  and  $w \in H^1(\Omega)$ . We have introduced an implicit Euler scheme for time differentiation, i.e., the first-order approximations:

$$\frac{\partial u^*}{\partial t^*} = \frac{u^{*,n+1} - u^{*,n}}{\Delta t^*}, \quad (2.17a)$$

$$\frac{\partial p^*}{\partial t^*} = \frac{p^{*,n+1} - p^{*,n}}{\Delta t^*}, \quad (2.17b)$$

which means that we need to solve the system (2.17) consecutively to complete the simulation time with a uniform grid  $[0, \Delta t, 2\Delta t, \dots]$ . A traditional Picard method is used to deal with the system non-linearities at each time-step, which will have a fixed error tolerance over the  $\ell^2$  norm for joint velocity and pressure of  $10^{-3}$ . Next, we recast the problem in finite dimension by means of the following standard Galerkin approach:

$$\begin{aligned} u^{*,n+1} &= \sum_{i=1}^N u_i^{*,n+1} \phi_i, \\ p^{*,n+1} &= \sum_{i=1}^N p_i^{*,n+1} \phi_i, \end{aligned} \quad (2.18)$$

where  $N$  is the number of nodes that discretize the working domain  $\Omega$ . To ease the reading, the same notation has been adopted for both the continuous and the discrete unknowns. The finite element method provides the solution of nodal coefficients  $u_i^{*,n+1}$  and  $p_i^{*,n+1}$  ( $i = 1, \dots, N$ ). We choose the same discretization space for both, velocity and pressure, namely, the piece-wise linear (lowest-order) space  $\mathbb{P}_1$  basis  $\phi_1, \dots, \phi_N$ . Then, it is easily shown that this approximation leads to the following matrix system of  $2N \times 2N$  equations:

$$\begin{bmatrix} (1 + \Delta t^* \frac{fRe}{16})M + \lambda_2 \Delta t^* C(u^{*,n}) & \Delta t^* B \\ \lambda_1 \Delta t^* B & M \end{bmatrix} \begin{bmatrix} u^{*,n+1} \\ p^{*,n+1} \end{bmatrix} = \begin{bmatrix} M u^{*,n} \\ M p^{*,n} \end{bmatrix} \quad (2.19)$$

where  $M \in \mathbb{R}^{N \times N}$  stands for a mass matrix with entries  $M_{ij} = \int_{\Omega} \phi_i \phi_j dx$ , the matrix  $B \in \mathbb{R}^{N \times N}$  for the coupling terms, with entries  $B_{ij} = \int_{\Omega} \phi_i \frac{\partial \phi_j}{\partial Z} dx$ , and the convection matrix  $C \in \mathbb{R}^{N \times N}$  with entries  $C_{ij} = \int_{\Omega} u^* \frac{\partial \phi_i}{\partial x^*} \phi_j dx$ . The integrals are computed with a standard Gaussian quadrature rule of three points per finite element. In addition, a classical fixed-point root-finder is utilized to solve for  $X_c$  in equation (2.12) for a given input Hedstrom number, thus allowing us to compute the yield stress and the adimensional constants  $\lambda_1$  and  $\lambda_2$ .

The assemblage of the matrices and the solver is handled with the in-house software MAD [46] (used already in several CFD works with finite elements, e.g. [47–51]), for finite elements and data assimilation, which supports CPU parallelization for optimal speed-up thanks to the underlying linear algebra library PETSc[52]. For this study, we use an AMD Epyc processor with 48 physical cores. We use the MUltifrontal Massively Parallel sparse direct Solver (MUMPs, [53, 54]) to compute the solutions of (2.19), .

The reader may remark the absence of stabilization techniques, as it is the gold standard for the discretization of the Navier-Stokes equations. In particular, we remark on the importance of the mass storage component  $(1/\Delta t^*)M$  in the second line of (2.19) as a regularizer that prevents the system of equations from getting close to singular. One should consider nonetheless that getting close to a divergence-free scenario may distort the condition number of the matrix in (2.19). On the other hand, it would be easy to counter a divergence-free situation. There are several stabilization techniques that would take this situation under control, such as the Brezzi-Pitkäranta approach [55], the streamline upwind Petrov-Galerkin one [56], or variational multi-scale methods [57]. The later will be explored in a fore-coming scientific study to test out unstable regimes ensuring numerical resolvability. In addition, the reader may notice that we follow a monolithic scheme for the problem unknowns. Other decoupling strategies for velocity and pressure for this application may be studied in forthcoming research [58].

### 3 Results

This section is devoted to study the numerical solutions of the transient slurry equations with convective effects. We first set up, in section 3.1 the necessary mesh and time step for the finite element scheme we employ so that we reach non-oscillatory or not excessively regularized solutions, as a quasi-convergence study. Next, in section 3.2, we inspect the numerical solution for a realistic parameter set that emulates copper-water mixture.



We then do a parametric study of the solutions including the effect of the fluid yield stress (section 3.3) and the impact of the valve closure time (section 3.4).

### 3.1 Convergence study

Let start testing out the solver convergence in space and time. To do so, we solve the governing dynamics for the set of parameters depicted in table 1, but considering  $\tau_y = 0$ , as it is the more challenging scenario from the numerical standpoint. For similar reasons, we also set a sudden closure for the valve, meaning that in the boundary conditions of (2.14) we set  $g(t) = 0$  at  $x = L$ . To study the mesh convergence, we narrow our attention to the pressure at a control point located at the valve. Consider a preliminary adimensional time step of  $10^{-6}$  and 4 meshes, with characteristic adimensional element sizes of  $10^{-2}$ ,  $2 \times 10^{-3}$ ,  $10^{-3}$ , and  $10^{-4}$ . We observe, in Figures 3.a and 3.b, a mesh independent solution up to  $\Delta x^* = 2 \times 10^{-3}$ , so we choose this element size for all the fore coming simulations. The critical jump is that of the wave onset, at the beginning of the simulation, so we zoom in the phenomena in Figure 3. For every simulation, we check how the reservoir pressure is recovered after the flow stops, as it is physically expected.

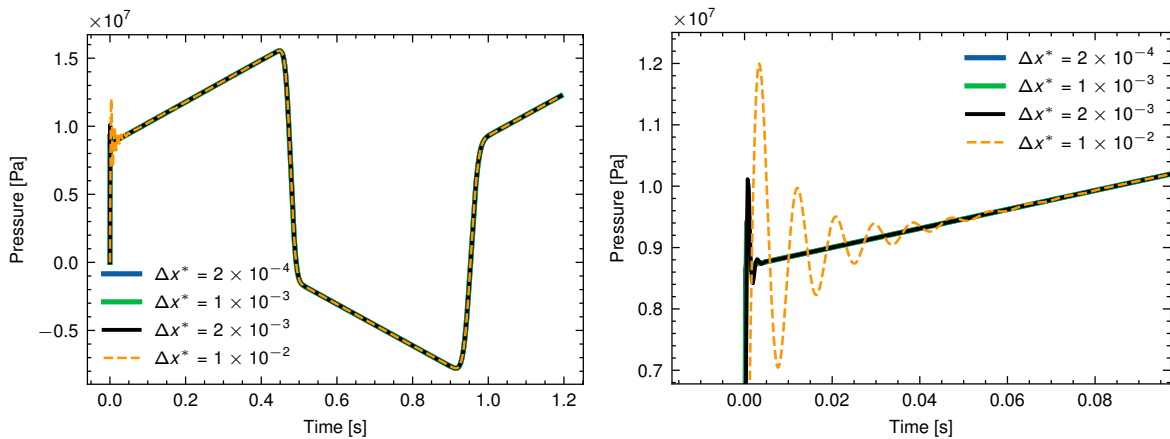


**Fig. 3** Mesh dependence test. As expected, the mesh refinement is critical after the instantaneous valve closure. This sets a threshold for the element size at  $\Delta x^* = 2 \times 10^{-3}$

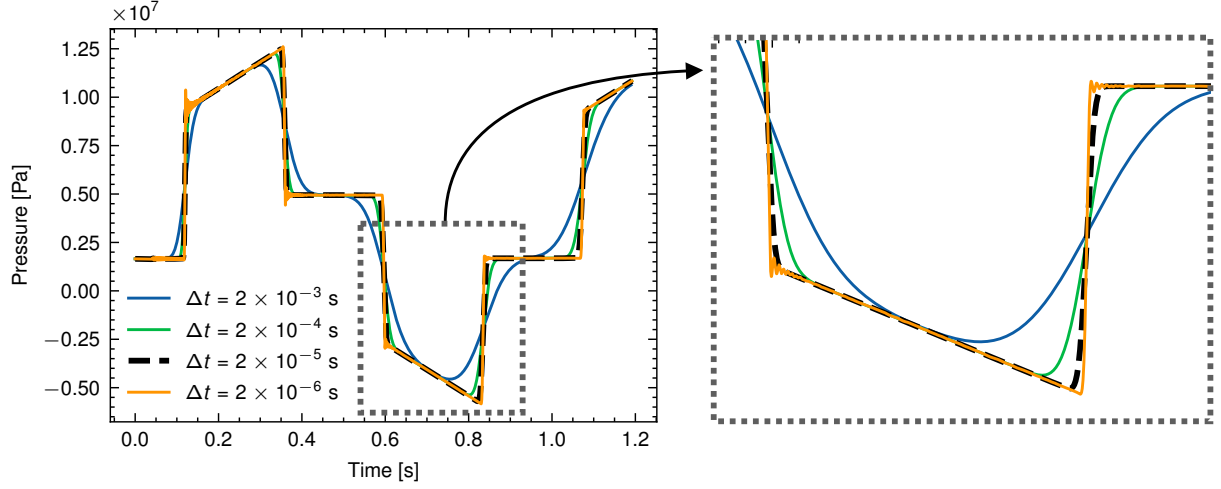
Similarly, the time step analysis in Figure 4.a shows that time steps over  $2 \times 10^{-3}$  s leads to excessively smooth solutions. This, and the fast Fourier transform of the solutions shown in Figure 4.b depicts a good frequency content preservation and solution behavior for a time step  $\Delta t^* = 10^{-4}$ , therefore we use it for all the simulations to come.

Concerning the solver performance, which in this test case boils down to invert 50000 systems of equations (one per time step) with 1001 degrees of freedom each, it takes a total simulation time of 66.34 seconds, using a single core of a 48 cores AMD Epyc processor.

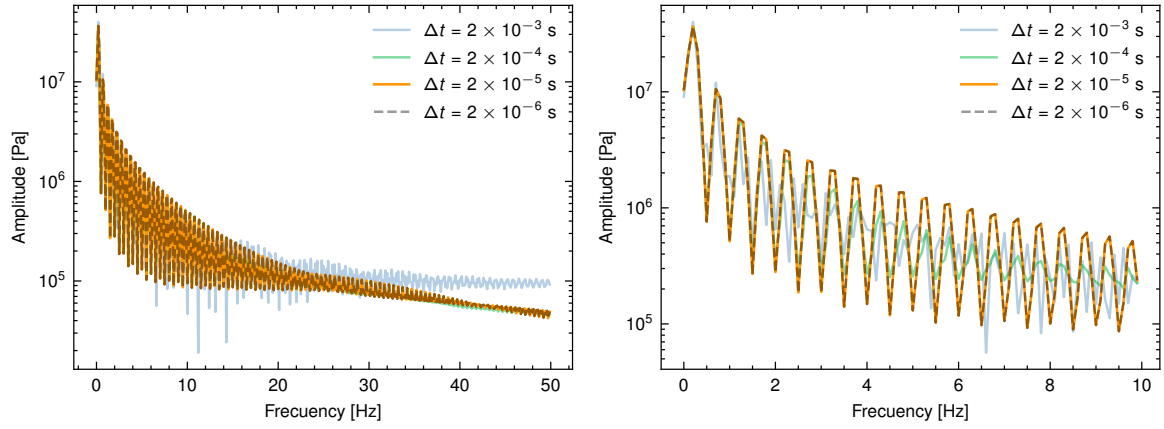
### 3.2 Simulation of a copper slurry

In this section we will apply the above system of equations to analyze the evolution of a hydraulic transient in a copper-water mixture pipeline system. This mixture is a homogeneous fluid, that is, a fluid whose solid concentration and velocity distribution can be considered practically uniform across the pipe diameter [15, 19]. This case is very important to the mining industry, especially in countries where mineral transport occurs through pipelines.

Table 1 shows the physical and mechanical properties for the slurry flow considered in this study, Table 2 the mixture density and bulk modulus and the expected theoretical values for the shockwave speed estimated according to the relations given by Eq.2.8 - Eq.2.10 for increasing values of  $C_V$ . Table 3 display the pipeline properties.



(a) Time domain



(b) Frequency domain

**Fig. 4** Convergence test for Newtonian case  $\text{He} = 0$ . This benchmark shows that  $\Delta t = 2 \times 10^{-5}$  s ( $\Delta t^* = 10^{-4}$ ) suffices to capture the hammer dynamics.

**Table 1** Physical and mechanical parameters for a copper slurry. Viscosity and yield stress data were extracted from [59]

Parameter	Meaning	Value
$\rho_s$	Solid density	8.9 g·cm <sup>-3</sup>
$\rho_f$	Liquid density (water)	1.0 g·cm <sup>-3</sup>
$K_f$	Liquid bulk modulus	2.1 GPa
$K_s$	Solids bulk modulus	140 GPa
$E$	Pipe elastic modulus (steel)	200 GPa
$\eta$	Slurry Bingham viscosity	≈ 0.03 Pa s
$\tau_y$	Slurry yield stress	≈ 26 Pa

**Table 2** Shockwave speeds ( $c$ ) for a copper tailing according to different authors. In the last column, overpressure values ( $\Delta P$ ) were included according to Joukowski formula  $\Delta P = \rho_m c_m u_o$

Concentration $C_V$	$\rho_m$ g·cm <sup>-3</sup>	$K_m$ GPa	Eq.2.8 m/s	Eq.2.9 m/s	Eq.2.10 m/s	$\Delta P$ MPa
10%	1.79	15.9	2979	1944	1042	5.07
15%	2.19	22.8	3229	1885	966	5.75
20%	2.58	29.7	3392	1808	911	6.39
25%	2.98	36.6	3506	1730	870	7.05
30%	3.37	43.5	3592	1658	840	7.71

Although in the range  $C_V > 30\%$  the mixture can still display a non-Newtonian behavior, a Bingham-like rheology will not be necessarily expected [15]. For higher concentrations, an hyper-concentrated flow regime can be reached that is characterized by a different rheological law (see *e.g.* [18]). In the same context, in the range  $C_V < 1\%$  a Newtonian-like regime is expected for the mixture, which can be addressed with usual methods [1, 2].

**Table 3** Parameter setting for the pipeline.  
The steel pipeline is class DN100, Sch.40s

Parameter	Meaning	Value
$L$	Pipe length	200.0 m
$H$	Reservoir height	100.0 m
$D$	Inner pipe diameter	102.3 mm
$e$	Wall thickness	6.0 mm
$P_A$	Allowable pressure	17.8 MPa

In agreement with authors experience in real engineering projects, results provided by Eqs. (2.8)-(2.9) are extremely large and then unrealistic. The wave speed values calculated from Eq.(2.10) can be considered most representative of a real transient event, in agreement with Kodura et al. [5-7]. Even more, it is expected that real values of the initial pressure surge are lower than theoretical estimations inspired on Joukowski's pressure scale, because of the lower shockwave speed (see *e.g.*, [5, 7]).

With all these elements, the pressure rise can be easily estimated as  $\Delta P = \rho_m c_m u_o$ . The last column of Table 2 shows some estimations of  $\Delta P$  by considering  $u_o = u_c = 2.72$  m/s a reference velocity. The maximum pressure values  $P_{max}$  obtained from numerical simulations can be later compared to the theoretical maximum pressure  $P_o + \Delta P$ , where  $P_o = \rho_m g H$  is the initial head static pressure. As expected, a risky situation for pipeline safety occurs when  $P_{max} \geq P_A$ , where  $P_A$  is the *maximum allowable pressure*. This last parameter is provided by the pipeline factory and it depends on wall schedule (see Table 3).

In Figure 5 we observe simulation snapshots during the phenomena onset after an instantaneous valve closure. In the figure, we show the system stationary initial condition, the over-pressure wave propagation, *i.e.* from the valve to the tank (at  $t = 0.1$  s) and the under-pressure, *i.e.*, from the tank to the valve (at  $t = 0.5$  s).

In addition, we show the temporal evolution of the numerical solutions for control points located at the tank ( $x = 0$ ), the pipe half length ( $x = L/2$ ), and the valve ( $x = L$ ), at Figures 6 and 7. We observe a rather slow friction dissipation and we check that the maximal numerical pressure reach a value of 13.86 MPa, which turns out to be surprisingly close to the factory allowable pressure  $P_A = 17.8$  MPa, but still ensuring a safe hammer wave propagation. The theoretical pressure rise discussed above, with more restricted assumptions, is lower than the numerical one, namely 11 MPa, yet in accordance with the obtained value.

### 3.3 Impact of the fluid yield stress

A comparison for several yield stress magnitudes is depicted in Figures 8 and 9. To convey this simulations, we have used the same parameter configuration as for the previous test case, but moving freely the Hedstrom number and thus recomputing the yield stress at each case. In these figures, we can see how larger Hedstrom numbers simulations depicts smaller peaks in over-pressure values, leading naturally to faster decay times. This is a natural an expected behavior, as it is intuitive that larger Hedstrom numbers will imply more difficulty to move the fluid in the first place so that the yield stress could be reached, thus leading to a damping effect seen in the overall dynamics.

We summarize this finding with Figure 10, where the maximal over-pressure for each simulation is shown against the corresponding Hedstrom number. We see how the plot range depicts almost twice overpressure values for the quasi-Newtonian case  $He = 10^3$ , with respect to  $He = 10^9$ .

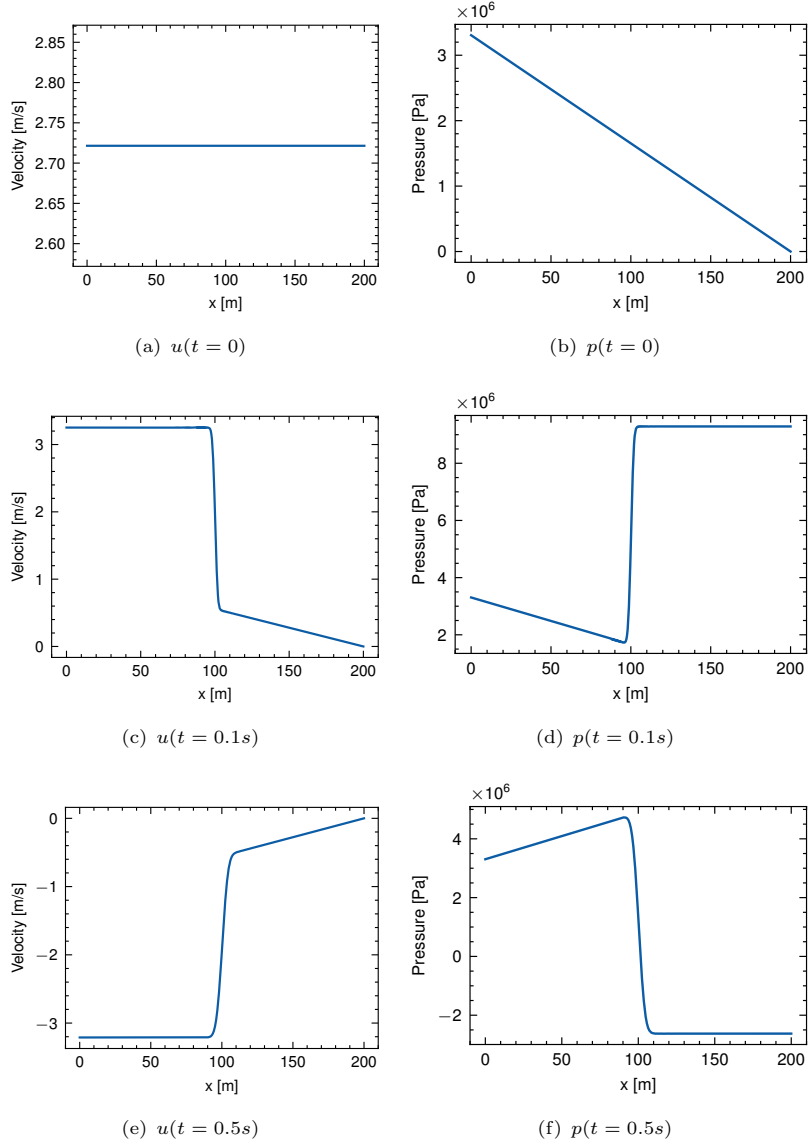


Fig. 5 Numerical solution snapshots at first wave cycle

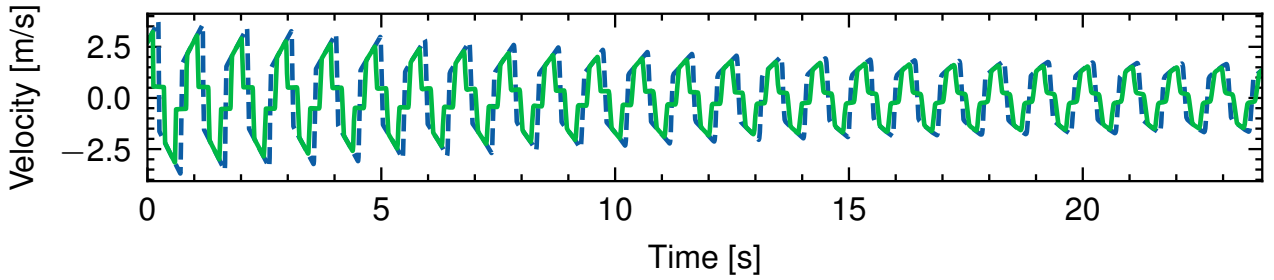


Fig. 6 Velocity for copper slurry on 2 control points, at  $x = 0$  (blue) and  $x = L/2$  (green)

### 3.4 Effects of the gradual valve closure

An additional brief test is performed to assess the impact of the gate closure model on the wave dynamics. We set the Dirichlet boundary condition in (2.14) as

$$g^*(t) = \frac{16}{f\overline{\text{Re}}} \left( 1 - \frac{t^*}{T_c} \right),$$

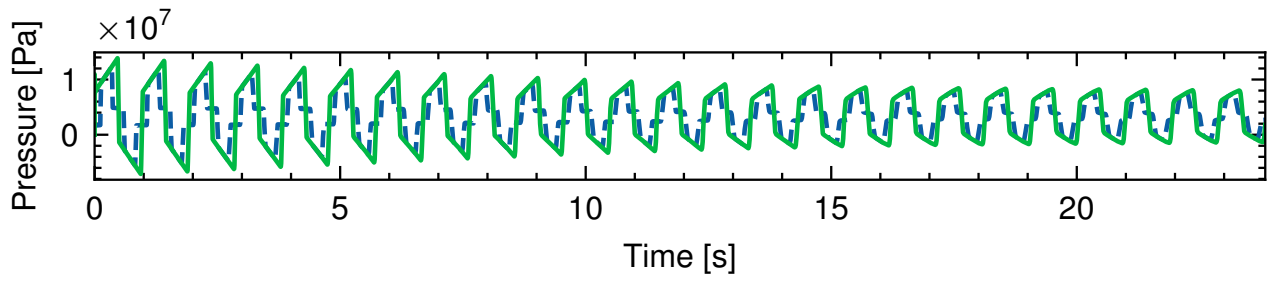


Fig. 7 Pressure for copper slurry on 2 control points, at  $x = L/2$  (blue) and  $x = L$  (green)

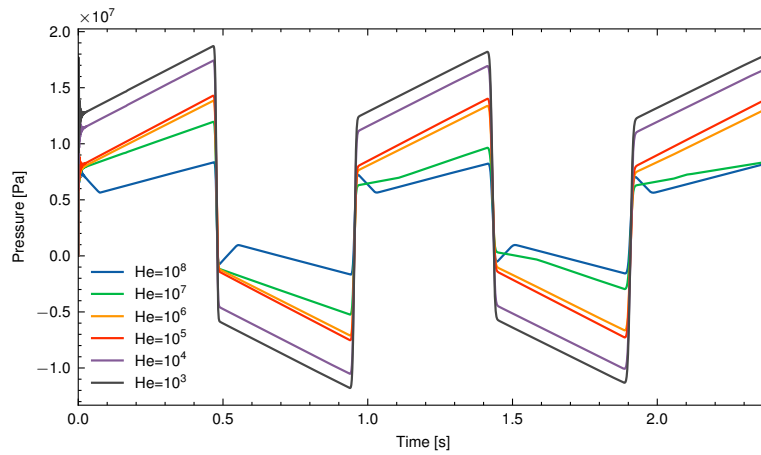


Fig. 8 Pressure evolution at valve control point, i.e.  $x = L$ .

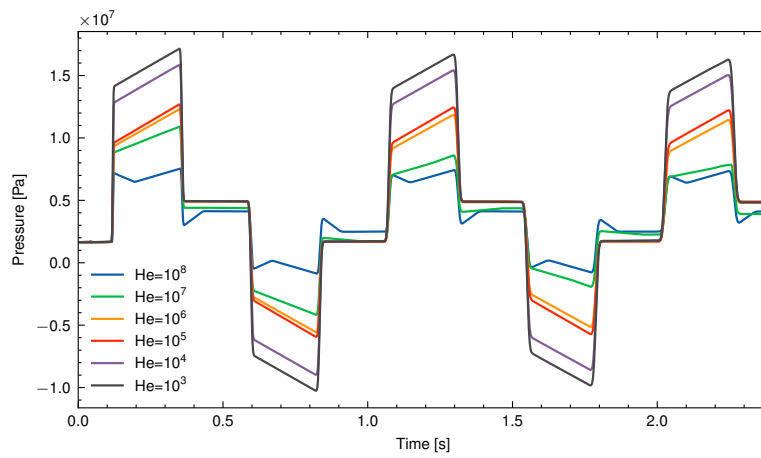


Fig. 9 Pressure evolution at half pipe control point, i.e.  $x = L/2$ .

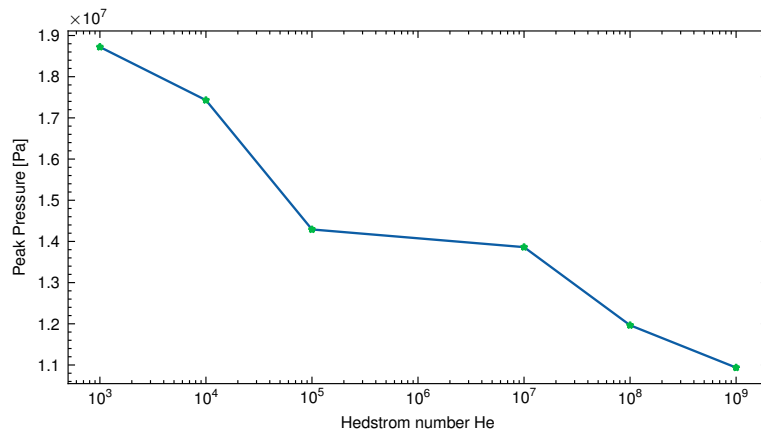
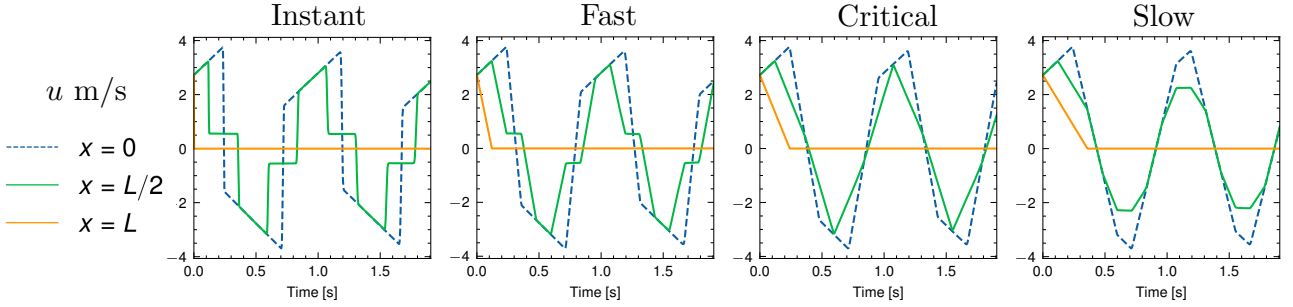
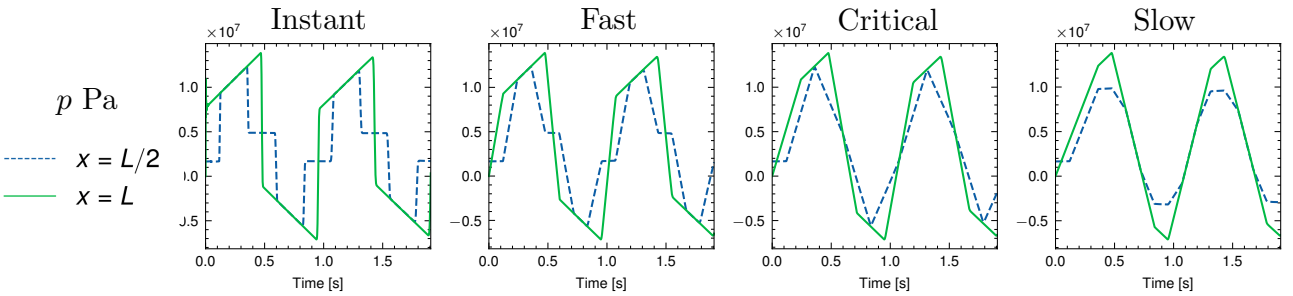


Fig. 10 Maximal over-pressure due to hammer effect against Hedstrom number.

where we check several closure times scaling it to the characteristic time  $L/c$ . The results, using the parametric configuration for the copper slurry, are shown in Figure 11 for velocity, and Figure 12, for the pressure. We depict four scenarios, namely an instant closure time ( $T_c = 0$ ), a fast closure time ( $T_c = 0.5$ ), a critical closure time ( $T_c = 1$ ) and a slow closure time ( $T_c = 1.5$ ). As expected, the sharpest numerical solutions of the governing equations are retrieved for the instantaneous closure, and we observe how the delay of the valve operation softens the overall dynamics, still keeping nonetheless similar over-pressure values. Yet, not-sudden pressure changes, as with the case  $T_c = 1.5$ , are preferable operation conditions.



**Fig. 11** Valve closure time impact on velocity evolution



**Fig. 12** Valve closure time impact on pressure evolution

The valve closure time study is summarized by looking at the plots of Figure 13, where we see how the overall simulation pressure peak (i.e. the first peak) behaves against both, the Hedstrom number, and the adimensional closure time. We first confirm that the Newtonian case brings higher pressure peaks, and we also see that the slow closure have a bigger consequence at the pipe half length control point. That is to say, at the valve closure control point, the peak pressure behavior is almost independent of the closure time, whereas at the middle control point, we observe a clear separation at the critical time  $T_c = 1$ , after which the pressure peak decreases almost linearly.

## 4 Conclusions

This study provides a comprehensive analysis of the pipeline hammer phenomenon in non-Newtonian Bingham plastic fluids, employing an efficient computationally inexpensive finite element method (FEM) to accurately simulate the transient dynamics. By integrating factors such as yield stress, convective effects, and varying valve closure times, this work advances the understanding of how non-Newtonian rheology affects pressure shockwaves in pipeline systems. The findings underscore some insights:

- **Impact of Yield Stress on Attenuation:** The yield stress in Bingham plastics contributes a damping effect, which facilitates faster attenuation of pressure peaks compared to Newtonian fluids. This effect is especially critical in applications where the reduction of peak pressures is essential for preventing pipeline stress and

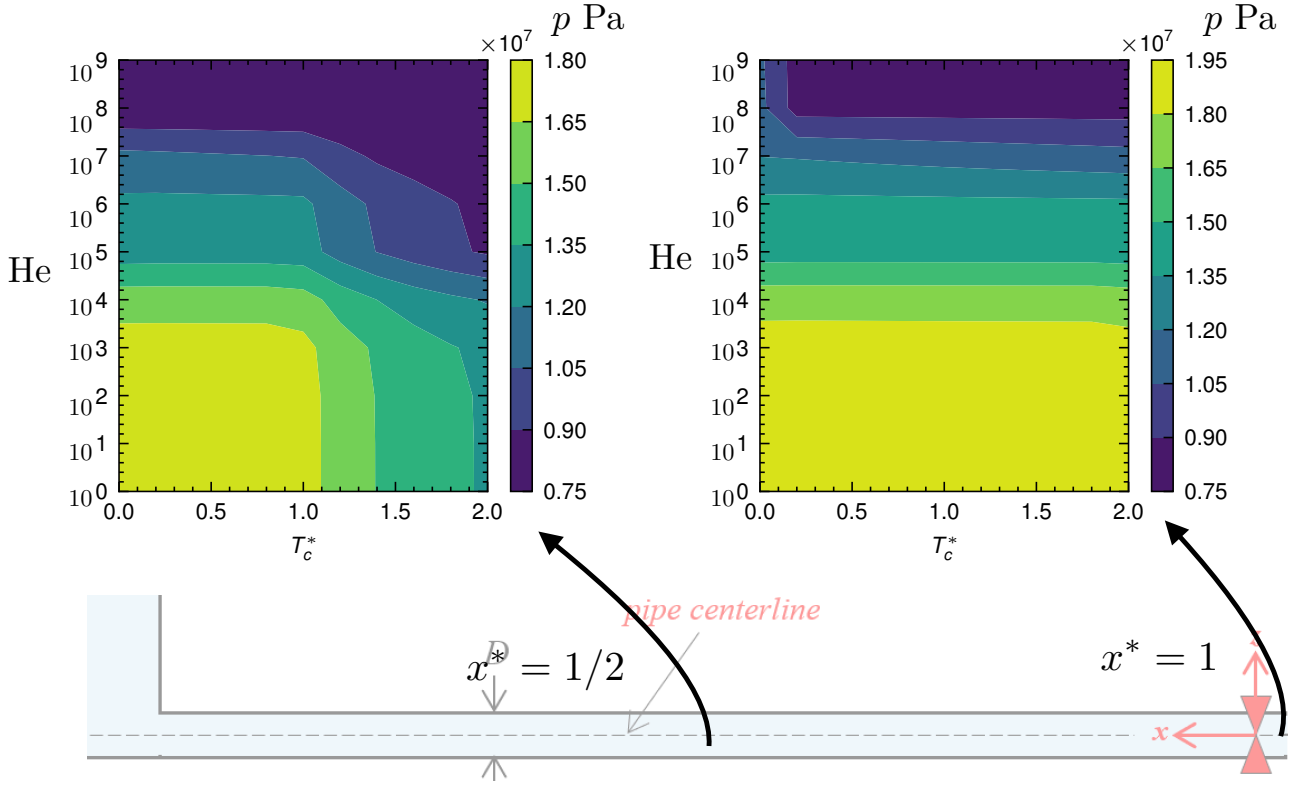


**Fig. 13** Parametric study for maximal pressure contours against valve closure time and Hedstrom number

material fatigue. As the yield stress increases, the number of pressure oscillations declines significantly, leading to enhanced stability within the system.

- **Valve Closure Dynamics:** The analysis of valve closure time revealed that gradual valve closures can lead to delayed, slightly slower, and smooth pressure wave and pressure peaks. The detailed parametric analysis summarized in Figure 13 shows how the peak pressure, a critical design quantity, behaves for a battery of configurations.
- **Adaptive Model for Laminar and Turbulent Flows:** The adaptive model used for both laminar and turbulent flow regimes demonstrated that hybrid approaches incorporating finite element schemes allow for accurate predictions across various flow conditions. This adaptability is essential when dealing with fluids that exhibit both Newtonian and non-Newtonian behaviors depending on flow rates and operational conditions, which contrast to regular studies [24] where laminar friction models are adopted even in high velocity conditions, as those usually reached in transient phenomena.

Overall, this work highlights the Bingham slurry parametric study, and also the advantages of using advanced numerical techniques, such as FEM, to accurately capture the complex interplay of rheological properties, flow dynamics, and operational changes in pipelines transporting non-Newtonian fluids. Future research could further refine these models through machine learning approaches for rapid parameter optimization, and stabilization techniques could be explored to enhance model robustness. This work lays a foundation for more resilient pipeline designs and informed operational strategies, particularly in industries where non-Newtonian fluids pose unique challenges to system stability and durability.

## Statements and Declarations

The authors declare no competing interest.

## References

- [1] Wylie, V.L. E.B.and Streeter: Fluid Transients. New York, USA (1978)
- [2] Chaudhry, M.H.: Applied Hydraulic Transients. Springer (2014). <https://doi.org/10.1007/978-1-4614-8538-4>
- [3] Ghidaoui, M.S.: On the fundamental equations of water hammer. Urban Water Journal **1**(2), 71–83 (2004) <https://doi.org/10.1080/15730620412331290001>
- [4] Ghidaoui, M.S., Zhao, M., McInnis, D.A., Axworthy, D.H.: A review of water hammer theory and practice. Appl. Mech. Rev. **58**(1), 49–76 (2005) <https://doi.org/10.1115/1.1828050>
- [5] Kodura, A., Kubrak, M., Stefanek, P., Weinerowska-Bords, K.: An experimental investigation of pressure wave celerity during the transient slurry flow. In: Free Surface Flows and Transport Processes: 36th International School of Hydraulics, pp. 259–269 (2018). Springer
- [6] Kodura, A., Weinerowska-Bords, K., Artichowicz, W., Kubrak, M., Stefanek, P.: In situ verification of numerical model of water hammer in slurries. Journal of Fluids Engineering **141**(8), 081115 (2019) <https://doi.org/10.1115/1.4042959>
- [7] Kodura, A., Weinerowska-Bords, K., Kubrak, M.: Simplified numerical model for transient flow of slurries at low concentration. Energies **15**(19), 7175 (2022) <https://doi.org/10.3390/en15197175>
- [8] Rocha, L., Oliveira, G., Negrao, C.O., Franco, A., Martins, A.: Modelling the start-up flow of well drilling fluids. Proceedings of ENCIT (2008)
- [9] Ihle, C.F.: Should maximum pressures in ore pipelines be computed out of system startups or power outages? Minerals Engineering **55**, 57–59 (2014) <https://doi.org/10.1016/j.mineng.2013.09.006>
- [10] Boger, D.V.: Rheology of slurries and environmental impacts in the mining industry. Annual Review of Chemical and Biomolecular engineering **4**, 239–257 (2013) <https://doi.org/10.1146/annurev-chembioeng-061312-103347>
- [11] Abdul-Wahab, S., Marikar, F.: The environmental impact of gold mines: pollution by heavy metals. Open Engineering **2**(2), 304–313 (2012) <https://doi.org/10.2478/s13531-011-0052-3>
- [12] Younger, P.L.: Environmental impacts of coal mining and associated wastes: a geochemical perspective. Geological Society, London, Special Publications **236**(1), 169–209 (2004) <https://doi.org/10.1144/GSL.SP.2004.236.01.12>
- [13] Cacciuttolo, C., Cano, D.: Environmental impact assessment of mine tailings spill considering metallurgical processes of gold and copper mining: case studies in the Andean countries of Chile and Peru. Water **14**(19), 3057 (2022) <https://doi.org/10.3390/w14193057>
- [14] Wahba, E.: Non-newtonian fluid hammer in elastic circular pipes: Shear-thinning and shear-thickening effects. Journal of Non-Newtonian Fluid Mechanics **198**, 24–30 (2013) <https://doi.org/10.1016/j.jnnfm.2013.04.007>
- [15] Baha Abulnaga, P.E.: Slurry Systems Handbook. McGraw-Hill Education (2021)
- [16] O'brien, J., Julien, P.: Physical properties and mechanics of hyperconcentrated sediment flows. Proc. ASCE HD Delineation of landslides, flash flood and debris flow Hazards (1985)



- [17] O'Brien, J.S., Julien, P.Y.: Laboratory analysis of mudflow properties. *Journal of hydraulic engineering* **114**(8), 877–887 (1988) [https://doi.org/10.1061/\(ASCE\)0733-9429\(1988\)114:8\(877\)](https://doi.org/10.1061/(ASCE)0733-9429(1988)114:8(877))
- [18] Julien, P.Y., Lan, Y.: Rheology of hyperconcentrations. *Journal of Hydraulic Engineering* **117**(3), 346–353 (1991) [https://doi.org/10.1061/\(ASCE\)0733-9429\(1991\)117:3\(346\)](https://doi.org/10.1061/(ASCE)0733-9429(1991)117:3(346))
- [19] Wasp, E.J., Kenny, J.P., Gandhi, R.L.: Solid-liquid flow: Slurry pipeline transportation [pumps, valves, mechanical equipment, economics]. *Ser. Bulk Mater. Handl.:(United States)* **1**(4) (1977)
- [20] Mitshita, R.S., Oliveira, G.M., Santos, T.G., Negrão, C.O.: Pressure transmission in yield stress fluids-an experimental analysis. *Journal of Non-Newtonian Fluid Mechanics* **261**, 50–59 (2018)
- [21] Pham, T.Q.D., Choi, S.: Numerical analysis of direct contact condensation-induced water hammering effect using openfoam in realistic steam pipes. *International Journal of Heat and Mass Transfer* **171**, 121099 (2021) <https://doi.org/10.1016/j.ijheatmasstransfer.2021.121099>
- [22] Darbhamulla, N.B., Jaiman, R.K.: A finite element framework for fluid–structure interaction of turbulent cavitating flows with flexible structures. *Computers & Fluids* **277**, 106283 (2024) <https://doi.org/10.1016/j.compfluid.2024.106283>
- [23] Wang, C., Nilsson, H., Yang, J., Petit, O.: 1d–3d coupling for hydraulic system transient simulations. *Computer Physics Communications* **210**, 1–9 (2017) <https://doi.org/10.1016/j.cpc.2016.09.007>
- [24] Oliveira, G.M., Franco, A.T., Negrão, C.O.R.: Mathematical Model for Viscoplastic Fluid Hammer. *Journal of Fluids Engineering* **138**(1), 011301 (2015) <https://doi.org/10.1115/1.4031001> [https://asmedigitalcollection.asme.org/fluidsengineering/article-pdf/138/1/011301/6194304/fe\\_138\\_01\\_011301.pdf](https://asmedigitalcollection.asme.org/fluidsengineering/article-pdf/138/1/011301/6194304/fe_138_01_011301.pdf)
- [25] Tawfik, A.: Air vessel sizing approach for pipeline protection using artificial neural networks. *Journal of Engineering and Applied Science* **70**(1), 34 (2023) <https://doi.org/10.1186/s44147-023-00206-8>
- [26] Brunton, S.L., Kutz, J.N.: *Data-Driven Science and Engineering: Machine Learning, Dynamical Systems, and Control*. Cambridge University Press (2019)
- [27] Fortier, A.: *Mécanique des Suspensions*. Masson (1967)
- [28] Adams, I., Simeonov, J., Bateman, S., Keane, N.: A bingham plastic fluid solver for turbulent flow of dense muddy sediment mixtures. *Fluids* **8**(6), 171 (2023) <https://doi.org/10.3390/fluids8060171>
- [29] De Oliveira, G.M., Rocha, L.L.V., Franco, A.T., Negrão, C.O.: Numerical simulation of the start-up of bingham fluid flows in pipelines. *Journal of Non-Newtonian Fluid Mechanics* **165**(19-20), 1114–1128 (2010) <https://doi.org/10.1016/j.jnnfm.2010.05.009>
- [30] Oliveira, G.M., Negrão, C.O., Franco, A.T.: Pressure transmission in bingham fluids compressed within a closed pipe. *Journal of Non-Newtonian Fluid Mechanics* **169**, 121–125 (2012) <https://doi.org/10.1016/j.jnnfm.2018.08.007>
- [31] Santos, T.G., Oliveira, G.M., Negrão, C.O.: Dimensionless analysis of non-Newtonian power-law fluid hammer. *Journal of Hydraulic Engineering* **149**(9), 04023034 (2023) <https://doi.org/10.1061/JHEND8.HYENG-13276>
- [32] White, F.M.: *Viscous Fluid Flow*. McGraw-Hill (1991)
- [33] Swamee, P.K., Aggarwal, N.: Explicit equations for laminar flow of bingham plastic fluids. *Journal of*

- [34] Darby, R., Melson, J.: How to predict the friction factor for flow of bingham plastics. *Chemical Engineering* (1981)
- [35] Tijsseling, A.S., Anderson, A.: *The joukowski equation for fluids and solids* (2006)
- [36] Tijsseling, A.S., Anderson, A.: Johannes von kries and the history of water hammer. *Journal of Hydraulic Engineering* **133**(1), 1–8 (2007)
- [37] Young, T.: Xiii. hydraulic investigations, subservient to an intended croonian lecture on the motion of the blood. *Philosophical Transactions of the Royal society of London* (98), 164–186 (1808)
- [38] Korteweg, D.J.: *Over voortplantings-snelheid van golven in elastische buizen*. Van Doesburgh, Netherlands (1878)
- [39] Korteweg, D.J.: Ueber die fortpflanzungsgeschwindigkeit des schalles in elastischen röhren. *Annalen der Physik* **241**(12), 525–542 (1878)
- [40] Thorley, A., Hwang, L.: Effects of rapid change in flowrate of solid-liquid mixtures. In: *Proceedings of Hydrotransport 6th Conference*, UK, pp. 229–242 (1979)
- [41] Han, W., Dong, Z., Chai, H.: Water hammer in pipelines with hyperconcentrated slurry flows carrying solid particles. *Science in China Series E: Technological Sciences* **41**, 337–347 (1998)
- [42] Assefa, K.M., Kaushal, D.R.: A comparative study of friction factor correlations for high concentrate slurry flow in smooth pipes. *Journal of Hydrology and Hydromechanics* **63** (2015)
- [43] Kerger, F., Archambeau, P., Erpicum, S., Dewals, B.J., Piroton, M.: An exact riemann solver and a godunov scheme for simulating highly transient mixed flows. *Journal of Computational and Applied Mathematics* **235**(8), 2030–2040 (2011) <https://doi.org/10.1016/j.cam.2010.09.026>
- [44] Zienkiewicz, O.C., Taylor, R.L., Zhu, J.Z.: *The Finite Element Method: Its Basis and Fundamentals*. Elsevier (2013)
- [45] Ern, A., Guermond, J.-L.: *Finite Elements I: Approximation and Interpolation*. Springer (2021)
- [46] Galarce Marin, F.: *Inverse problems in hemodynamics. fast estimation of blood flows from medical data*. <https://gitlab.com/felipe.galarce.m/mad/>. PhD thesis, INRIA Paris & Laboratoire Jacques-Louis Lions. Sorbonne Université (2021)
- [47] Galarce, F., Lombardi, D., Mula, O.: Reconstructing haemodynamics quantities of interest from Doppler ultrasound imaging. *Int. J. Numer. Meth. Biomedical Eng.* (2021) <https://doi.org/10.1002/cnm.3416>
- [48] Galarce, F., Tabelow, K., Polzehl, J., Panagiotis, C.P., Vavourakis, V., Lilaj, L., Sack, I., Caiazzo, A.: Displacement and pressure reconstruction from magnetic resonance elastography images: Application to an in silico brain model. *SIAM Journal on Imaging Science* (2023) <https://doi.org/10.1137/22M149363X>
- [49] Galarce, F., Mura, J., Caiazzo, A.: Bias and multiscale correction methods for variational state estimation. *Applied Mathematical Modelling* **138**, 115761 (2025) <https://doi.org/10.1016/j.apm.2024.115761>
- [50] Galarce, F., Lombardi, D., Mula, O.: State estimation with model reduction and shape variability. application to biomedical problems. *SIAM Journal on Scientific Computing* **44** (2022) <https://doi.org/10.1137/21M1430480>

- [51] Galarce, F., Pacheco, D.: Fully consistent lowest-order finite element methods for generalised stokes flows with variable viscosity. ArXiv preprint (2024)
- [52] Balay, S., Abhyankar, S., M.D., A., Brown, J., Brune, P., Buschelman, K., Dalcin, L., Eijkhout, V., Gropp, W.D., Kaushik, D., Knepley, M.G., McInnes, L.C., Rupp, K., Smith, B.F., Zampini, S., Zhang, H.: PETSc Web page (2015). <http://www.mcs.anl.gov/petsc>
- [53] Amestoy, P.R., Duff, I.S., L'Excellent, J.-Y.: Multifrontal parallel distributed symmetric and unsymmetric solvers. *Computer Methods in Applied Mechanics and Engineering* **184**(2), 501–520 (2000) [https://doi.org/10.1016/S0045-7825\(99\)00242-X](https://doi.org/10.1016/S0045-7825(99)00242-X)
- [54] Amestoy, P.R., Duff, I.S., L'Excellent, J.-Y., Koster, J.: A fully asynchronous multifrontal solver using distributed dynamic scheduling. *SIAM Journal on Matrix Analysis and Applications* **23**(1), 15–41 (2001) <https://doi.org/10.1137/S0895479899358194>
- [55] Brezzi, F., Pitkaranta, J.: On the stabilization of finite element approximations of the stokes equations. *Efficient Solutions of Elliptic Systems* (1984)
- [56] Tezduyar, T.E.: Stabilized finite element formulations for incompressible flow computations **28**, 1–44 (1991) [https://doi.org/10.1016/S0065-2156\(08\)70153-4](https://doi.org/10.1016/S0065-2156(08)70153-4)
- [57] González, A., Castillo, E., Cruchaga, M.A.: Numerical verification of a non-residual orthogonal term-by-term stabilized finite element formulation for incompressible convective flow problems. *Computers & Mathematics with Applications* **80**(5), 1009–1028 (2020) <https://doi.org/10.1016/j.camwa.2020.05.025>
- [58] Guermond, J., Mineev, P., Shen, J.: An overview of projection methods for incompressible flows. *Computer Methods in Applied Mechanics and Engineering* (2005) <https://doi.org/10.1016/j.cma.2005.10.010>
- [59] Alejo, B., Barrientos, A.: Model for yield stress of quartz pulps and copper tailings. *International Journal of Mineral Processing* **93**(3-4), 213–219 (2009) <https://doi.org/10.1016/j.minpro.2009.08.002>